Chapter 1

I-III-VI_2 Chalcopyrite Compound Semiconductors

The chalcopyrite compound $CuInS_2$ and alloys of the $CuInS_2$-$CuGaS_2$ system have been used as absorber layers for thin film solar cells in this work. This chapter starts with a brief description of the material properties of Cu-chalcopyrites. The basic principles of a photovoltaic device are then introduced and the current-voltage characteristics are discussed. Special emphasis is laid on the recombination in heterojunction solar cells based on Cu-chalcopyrites and their influence on the attainable open circuit voltage under illumination.

1.1 Material Properties

A first fundamental work about the growth and the structural characterization of chalcopyrite compounds was published by Hahn et al. in 1953 [15]. Later work on chalcopyrites was mostly motivated by their potential for non-linear optical applications, visible-light emitters, and photodetectors [16–19].

In the beginning of the seventies a first comprehensive review of chalcopyrite compounds was given in the book by Shay and Wernick [20]. Later, Pamplin published several reviews about phase formation rules, thermodynamic phase relations, and experimental results of ternary adamantine compounds, among them the Cu-chalcopyrites [21, 22]. Whereas earlier work was almost entirely about single crystal specimen, more recent experimental investigations have been focused on thin films, due to the high potential of these materials for large area photovoltaic modules.

1.1.1 Crystal Structure

$CuInS_2$ belongs to the group of ternary chalcopyrite compounds which derives from the group IV class of tetrahedrally bonded semiconductors according to the Grimm-Sommerfeld rule, i.e. there must be an average of 4 valence atoms per atomic site. In these structures

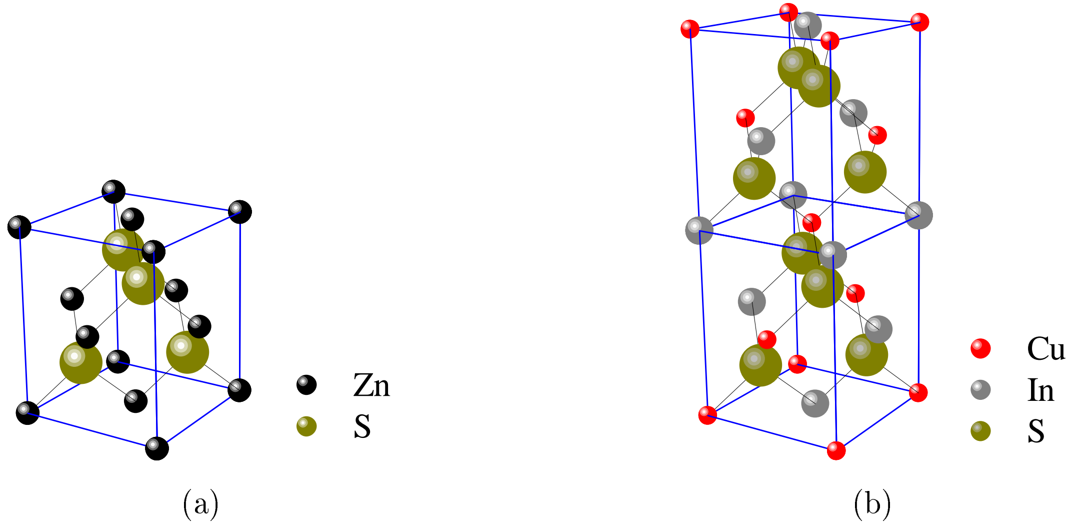

Figure 1.1: Crystal structure of (a) zincblende and (b) chalcopyrite lattice.

each atom has four neighbors arranged at the corners of a regular tetrahedron bonded by sp^3 bonds. The tetrahedral structure of the chalcopyrites can be considered as a superlattice structure of the sphalerite or zincblende structure which has a diamond like structure (such as Si) consisting of two inter-penetrating face centered cubic lattices, separated by a translation vector of $(\frac{1}{4},\frac{1}{4},\frac{1}{4})$. One sublattice is occupied by cations and the other by anions (II-VI and III-V compounds). In a ternary chalcopyrite the cations are furthermore replaced by a one cation of higher valency and one cation of lower valency which occupy the cation sublattice in an ordered manner as shown in Figure 1.1 (b). In that sense $CuInS_2$ can be envisioned as the ternary analogue of the binary ZnS. The reduced symmetry, due to the two kinds of cations, leads to a primitive cell of eight atoms in the chalcopyrite structure compared to a primitive cell of two atoms in the zincblende structure. The Bravais lattice of the chalcopyrite is body centered tetragonal. Compared to the face centered cubic Bravais-cell of the zincblende the unit cell is doubled along the crystal c axis. If the different cations are distributed at random, the ternary compound has a sphalerite structure.

Each S atom in the lattice is at the center of a tetrahedron with four cations at each corner. Since in a chalcopyrite structure, in contrast to the zincblende, the sulfur atom is bonded to two types of cations the respective bond lengths are not necessarily identical. As a result the tetrahedron is no longer regular but is distorted along the crystal c-axis such that the c/a ratio deviates from the ideal value of 2.0 (Figure 1.2). In addition, the difference in bonding length leads to an internal displacement of the anion away from the ideal position $0.25\,a$ so that the anion sublattice is slightly distorted. In the case of $CuInS_2$ the Cu-S bond length is 2.335 Å, whereas the In-S bond length is 2.464 Å [23]. As a result the sulfur atom moves away from the In-atoms and towards the Cu-atoms resulting in a stretched unit cell with a c/a ratio of 2.014 [8]. In the case of the $CuGaS_2$

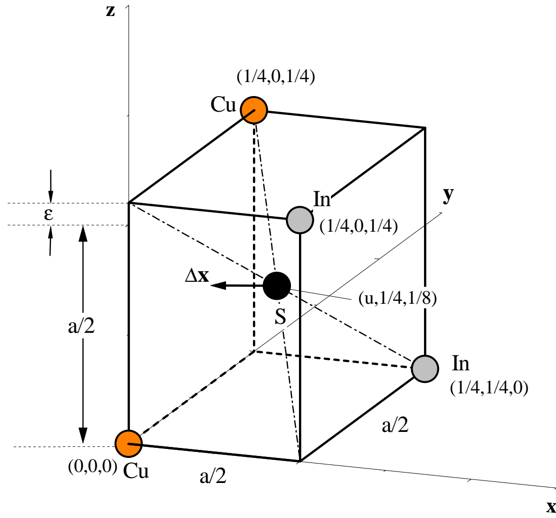

Figure 1.2: Tetrahedron distortion in $CuInS_2$. ϵ denotes the tetragonal distortion of the unit cell along the crystal c axis.

lattice the Ga-S bond is shorter than the Cu-S bond, hence the unit cell is compressed with a c/a ratio = 1.97 [8]. Precise X-ray diffraction measurements of $CuInS_2$ and $CuGaS_2$ crystals were performed by Abrahams and Bernstein [23] at samples grown from the melt and by Spiess et al. [24] at samples synthesized by halogen vapor transport reaction. The determined lattice parameters are listed, together with the values of the early work of Hahn et al. [15] in Table 1.1

Table 1.1: Lattice parameters of $CuInS_2$ and $CuGaS_2$ single crystals as determined by Hahn et al. [15], Abrahams and Bernstein [23], and Spiess et al. [24]. The u values refers to the x-coordinate of the sulfur atom (see Figure 1.2).

Compound	$a = b$ (nm)	c (nm)	c/a	u	Ref.
$CuGaS_2$	0.5349	1.047	1.958	0.25	[15]
	0.534741(7)	1.047429(6)	1.95876	0.2539(4)	[23]
	0.5356(1)	1.0435(5)	1.948	0.275(5)	[24]
$CuInS_2$	0.5517	1.106	2.005	0.20	[15]
	0.552279(7)	1.113295(22)	2.01582	0.2295(4)	[23]
	0.5523(4)	1.112(2)	2.013	0.214(7)	[24]

In a similar fashion as the ternary chalcopyrite compounds can be derived from its binary analogons it is possible to further substitute an additional metal M in a ternary $A^{I}B^{III}X_2^{VI}$ compound without violating the four electrons per lattice site rule. In general in the case of an isovalent substitution, e.g. $A^{I}B^{III}_{1-x}M^{III}_{x}X_2^{VI}$ (M substitutes for B), the new quaternary compound will still be a chalcopyrite, whereas a non-isovalent substitution will be accommodated in the crystal lattice by the formation of associated vacancies (defect chal-

copyrite compounds), e.g. $A^{I}_{1-2x}M^{II}_{x}\Box_{x}B^{III}X^{VI}_{2}$ (M substitutes for A with cation vacancies). A discussion of the vast range of substitutions and solid solution possibilities which still crystallize in a tetrahedrally bonded structure can be found in [21]. Complete solid solubility and mixed crystal formation have been reported for ternary chalcopyrite systems such as $CuInSe_2$-$CuGaSe_2$ and $CuInS_2$-$CuGaS_2$ (see Ref. in [22]), which due to their band gaps in the region of 1.0 eV → 2.4 eV and their high absorption coefficients are ideal materials for solar cell applications. Whereas fundamental electronic properties such as type of conductivity, are not affected by the alloy formation the usually observed gradual change in properties like lattice parameters, band gap and refractive index with alloy composition offers the possibility of tailoring these semiconducting materials to the specific needs of a device.

This work focues on the iso-valent substitution of In by Ga in $CuInS_2$ thin films. Solid solutions of $CuInS_2$ and $CuGaS_2$ have been grown and characterized by several authors [25–30]. The compositional dependences of the lattice constant a and c (Figure 1.3) or band gap energy (see next section) obeys Vegard's law [31], i.e. they vary linearly between the lattice constants of the *end point* materials $CuInS_2$ and $CuGaS_2$.

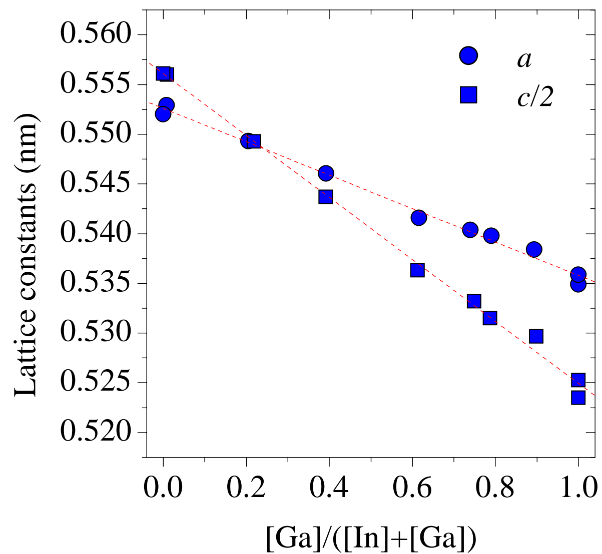

Figure 1.3: Lattice constants a and $c/2$ of the $CuInS_2$-$CuGaS_2$ alloy system (from Ref. [25]).

1.1.2 Phase Equilibria

In order to understand the phase formation of ternary I-III-VI_2 compounds their phase equilibria can be discussed in terms of temperature or composition. The ternary compositional triangle is the basis for analyzing the composition dependent phase behavior of these materials. In Figure 1.4 such a schematic ternary phase diagram for $CuInS_2$ is shown. A more detailed ternary phase diagram of $CuGaS_2$ can be found in Appendix A.5. For the sake of clarity only the pseudo binary lines Cu_2S-In_2S_3 and CuS-InS are indicated in the diagram. To describe the composition $I_xIII_yVI_z$, of a point within the ternary field

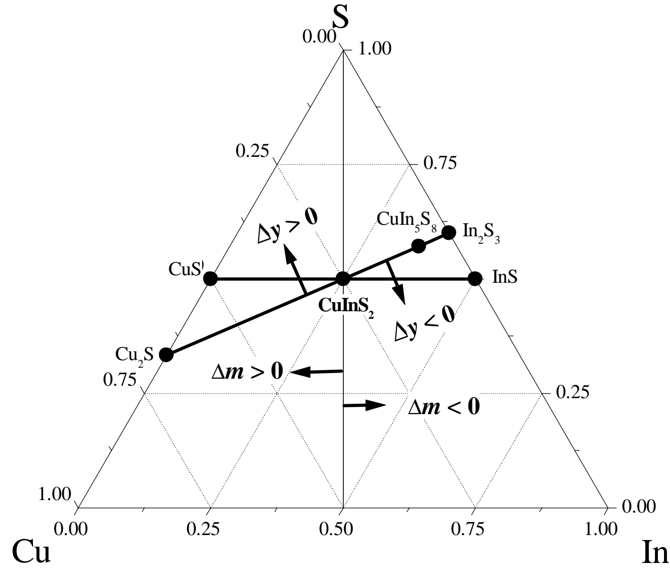

Figure 1.4: Schematic ternary phase diagram of $CuInS_2$˙

relative to the composition of the chalcopyrite Groenick and Janse [32] have introduced two independent parameters, i.e. the deviation in molecularity Δm and the deviation in valence stoichiometry Δy:

$$\Delta m = \frac{x}{y} - 1\,, \quad \Delta y = \frac{2z}{x+3y} - 1\,, \tag{1.1}$$

where x, y, and z are the atomic concentrations of the individual atoms. As indicated in Figure 1.4 Δy describes compositional deviations from the pseudo binary Cu_2S-In_2S_3 line, where $\Delta y < 0$ corresponds to anion poor and $\Delta y > 0$ to anion rich material. Δm divides the triangle into Cu-rich and Cu-poor compositions. As was shown by Binsma [33] changes in Δm along the Cu_2S-In_2S_3 line ($\Delta y = 0$) play a major role in fixing the defect-chemical state of the compound, however they do not change the type of conductivity of the chalcopyrite, rather, it is Δy, the deviation in stoichiometry, that is reflected in the electrical properties and affects the level and sign of doping. In other words the electronic properties of Cu-chalcopyrites such as type of conductivity, carrier concentration and mobility are mainly determined by intrinsic defects. Here sulfur vacancies lead to donor levels whereas cation vacancies will cause acceptor levels. This could be experimentally verified as annealing of $CuInS_2$ crystals in the presence of sulfur leads to p-type conductivity and annealing in the presence of In leads to n-type conductivity [34]. In thin film deposition of chalcopyrite layers the chalcogen is generally offered in over-stoichiometric amounts, hence the films normally exhibit p-type conductivity. However, it has been shown that the high vapor pressure of sulfur compared to e.g. selenium at film growth temperatures imposes a kinetic limitation onto the adsorbtion of sulfur from the gas phase [35], which can result in a high number of compensating donors. As a result the free carrier density drops by several orders of magnitude between $CuInSe_2$ and $CuInS_2$ [36]. It was shown

by several authors that the incorporation of Na and/or Ga in $CuInSe_2$ thin films has beneficial effects on the incorporation of the chalcogen, thereby significantly widening the processing window for device grade material of *p*-type conductivity [37]. Experimental results reported by Walter [36] indicated a similar effect for $CuIn(S,Se)_2$ (Figure 1.5). Whereas the carrier concentration in $CuIn(S,Se)_2$ thin films drastically drops when the selenium/sulfur ratio of the gas phase is lowered (due to the above mentioned kinetic limitation for sulfur incorporation) the carrier concentration remains almost unaffected by the changing chalcogen composition in the gas phase if some of the In is replaced by Ga (Figure 1.5).

In this work the investigated growth regime relies on a Cu-rich preparation process, where an additional Cu-S phase segregates during thin film formation. The growth assistance by a copper-chalcogen binary phase is another way of overcoming the kinetic limitation for sulfur incorporation [38]. Thin films prepared in the course of this work always exhibit p-type conductivity and carrier densities around $10^{17}\,cm^{-3}$.

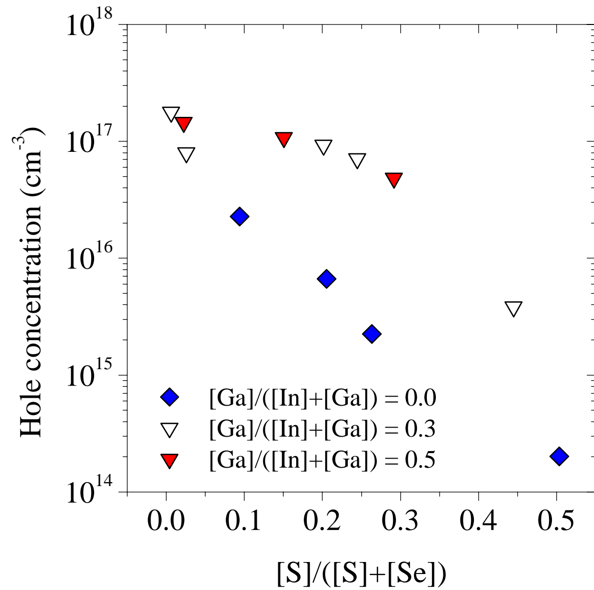

Figure 1.5: Carrier density as a function of [S]/([S]+[Se]) ratio in $Cu(In,Ga)(S,Se)_2$ thin films of different [Ga]/([In] + [Ga]) ratio (from Ref. [36]).

1.1.3 Electronic Band Gap of $Cu(In_{1-x}Ga_x)S_2$

The electronic band structure of a chalcopyrite compound can in principle be derived from its II-VI analogue since in both structures (zincblende and chalcopyrite) the chemical binding is realized via hybrid sp^3-orbitals. The resulting band structure at the Γ-point is determined by a s-type conduction band and a p-type valence band [39].

However, it was shown that the uppermost valence bands of a I-III-VI$_2$ compound are largely influenced by the d-levels of the group I metal in the valence band [40]. As a consequence the valence band is split into three single bands due to spin-orbit interaction

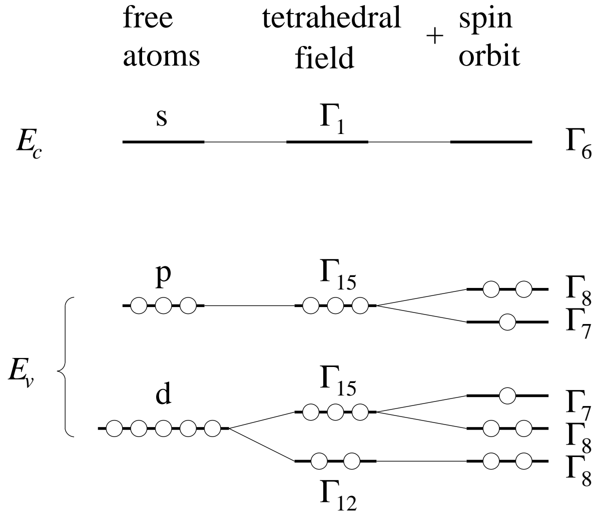

Figure 1.6: Qualitative sketch of the behavior of d-levels in a tetrahedral field (after Ref. [40]).

and due to the crystal field in the tetragonal structure (Figure 1.6). The interaction between the Γ_{15} levels in Figure 1.6 will raise the uppermost Γ_{15} to higher energies, so that the direct band gap at the Γ-point of a chalcopyrite is in general 1 eV lower than the value of the respective II-VI compound. Theoretical calculations by Jaffe and Zunger [9] revealed that the reduced band gap in chalcopyrites can be explained by two effects - a chemical effect $\Delta E_g^{\mathrm{chem}}$ which is due to the p-d hybrids and a structural $\Delta E_g^{\mathrm{struc}}$ which is related to the anion displacement in the chalcopyrite lattice.
The first direct transition in $CuGaS_2$ occurs at 2.40 eV (binary analogue ZnS, $E_g = 3.77$ eV) and in $CuInS_2$ at 1.53 eV ($(Cd_{0.5}Zn_{0.5})S$ $E_g = 3.1$ eV) [39]. Spin orbit interactions accounts for a splitting of ≈ 12 meV of the valence band in both compounds. However, the expected additional splitting due to the tetragonal field vanishes in $CuInS_2$ which leads to a doubly degenerated valence band (Γ_8 in Figure 1.6) which lies below the non-degenerated band (Γ_7). The addition of Ga to $CuInS_2$ lifts the partial degeneracy. According to Tell et al. [41] the crystal-field splitting in the $Cu(In_{1-x}Ga_x)S_2$ alloy varies nearly linearly with x from zero in $CuInS_2$ to -130 meV in $CuGaS_2$. Figure 1.7 plots the compositional dependence of experimentally determined transition energies due to the first direct band gap in the alloy system $Cu(In_{1-x}Ga_x)S_2$ as measured by several authors. Although absolute energy values differ quite significantly between different reports all groups found a slightly non-linear dependence of the band gap on composition. The increase in the major splitting of the valence bands with increasing amount of Ga in the alloy can clearly be seen.

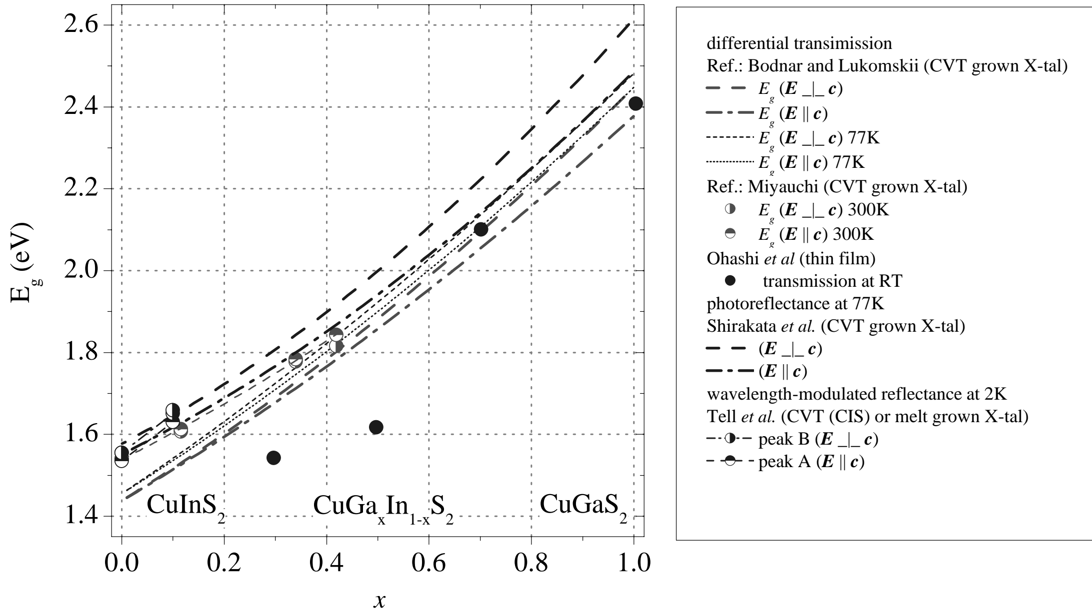

Figure 1.7: Compositional dependence of transition energies due to the first direct band gap in the system $Cu(In_{1-x}Ga_x)S_2$ (Ref.: Miyauchi et al. [26], Tell et al. [41], Bodnar et al. [28], Shirakata et al. [42], Ohashi et al. [43])

1.2 Solar Cells

Photovoltaic energy conversion relies on the internal photovoltaic effect according to which an incident photon can transform its energy to an electron in a solid. In a semiconductor this leads to the absorption of an incoming photon flux by excitation of electrons across the forbidden gap, provided the photon energy $h\nu$ is greater then the band gap energy E_g. In general the excited electrons will recombine with a hole after a material specific life time. However, in a solar cell the light generated electron-hole pairs are spatially separated, e.g. by the internal electrical field of a *p*-*n* junction, before they can recombine. The resulting electrical potential can then be utilized to drive an electrical load.
The current transport across a *p*-*n* junction is characterized by two currents; the drift current caused by the electrical field in space charge region of the junction and the diffusion current which flows in the opposite direction and which is driven by the concentration gradient of the charge carriers across the junction. In thermal equilibrium (i.e. no external voltage) the currents cancel out each other. If an external voltage is applied at the junction the *j*-*V* characteristics can be described by an analytical solution found by Shockley in

1949 [44], the so-called *ideal-diode equation*:

$$j(V) = j_{01}\left[\exp\left(\frac{V}{V_T}\right) - 1\right] , \tag{1.2}$$

where

$$j_{01} = \left(\frac{qD_p}{L_p}p_n + \frac{qD_n}{L_n}n_p\right) .$$

Here, ideal diode means that no parasitic series or shunt resistances are taken into account and that the recombination of charge carriers within the space charge region of the p-n junction is neglected. In Equation (1.2) j_{01} refers to the saturation current density, which is determined by specific material properties of the semiconductors constituting the junction; the minority carrier concentrations p_n and n_p, the diffusivities D_n and D_p and the diffusion lengths $L_x = \sqrt{D_x \tau_x}$ in emitter and base; τ_x is the minority carrier lifetime. $V_T \equiv \frac{kT}{q}$ is the thermal voltage.
As mentioned above under illumination excess charge carriers are generated in the solar cell. These non-equilibrium carriers will either recombine or they will be separated by the internal field in the space charge region, thereby causing an additional current density, the light generated or photo current j_{ph}, superimposed onto the diode current density, hence

$$j(V) = j_{01}\left[\exp\left(\frac{V}{V_T}\right) - 1\right] - j_{ph} . \tag{1.3}$$

Here the light generated current is assumed to be independent of the voltage across the junction.

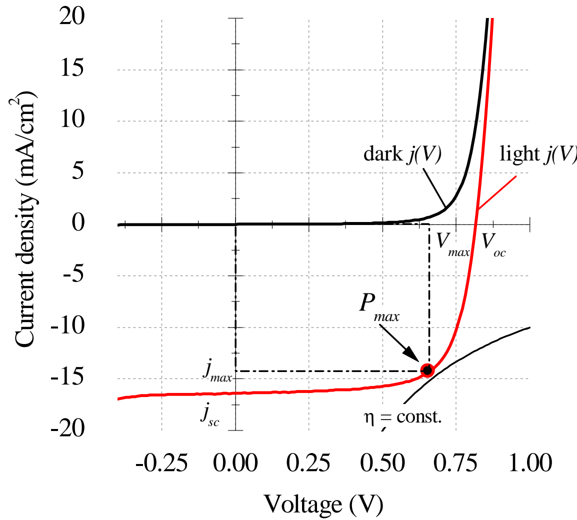

Figure 1.8: j-V characteristics of a solar cell.

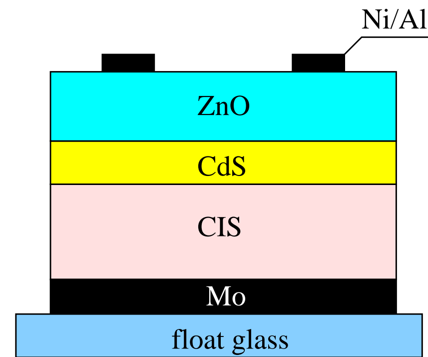

Figure 1.9: Structure of chalcopyrite thin film solar cell (not to scale).

The maximum power which can be extracted from a photovoltaic solar cell is determined by the rectangle of maximum area inscribed in the j-V curve (Figure 1.8), where j_{max} and

V_{max} are the current density and the voltage at the maximum power point, respectively. The efficiency η of the solar cell can be defined as

$$\eta = \frac{ff \times j_{sc} \times V_{oc}}{P}\,, \tag{1.4}$$

where P refers to the incident power, j_{sc} to the current density under short circuit ($V = 0$), and V_{oc} to the voltage under open circuit ($j_{sc} = 0$). ff, which is referred to as the fill factor, describes the shape of the j-V characteristics and is given by

$$ff = \frac{j_{max} \times V_{max}}{V_{oc} \times j_{sc}}\,. \tag{1.5}$$

1.2.1 Chalcopyrite Heterojunction Solar Cells

A typical chalcopyrite thin film solar cell consists of a heterojunction formed by a chalcopyrite p-type absorber layer and a transparent n-type window layer.
Figure 2.1 on page 22 depicts the layer sequence of a chalcopyrite heterojunction solar cell. A Mo coated float glass serves as the substrate. The Mo layer is about one micron thick and is used as the back contact. The light absorbing layer, which is deposited onto the Mo-back contact is formed by a chalcopyrite thin film. The heterojunction is completed by a thin (50–80 nm) n-type CdS buffer layer and a n/n^+-type ZnO bilayer. For laboratory scale devices an additional Ni/Al front grid is deposited as a front contact. The CdS and ZnO layers have an optical band gap of 2.4 eV and 3.2 eV, respectively. They are therefore transparent for almost all of the incident sun light. The ZnO layers are referred to as the window. Typical absorber layer materials currently used are $CuInSe_2$, $CuInS_2$, $CuGaSe_2$ and their alloys. Due to the high absorption coefficients of these materials layer thicknesses of 2–3 μm are sufficient to absorb all of the incident sun light. The highest efficiencies are currently achieved with solar cells based on $Cu(In_{1-x}Ga_x)Se_2$ alloys ($x \approx 0.2$). Details on the preparation sequence used to fabricate devices in this work will be given in Section 2.1.

Since the current collecting junction is formed by different semiconductor materials, i.e. absorber, buffer and window, band discontinuities will occur at the interface. Depending on the conduction band off set ΔE_c at the interface there are two types of heterojunctions; $\Delta E_c > 0$ is referred to as Type-I or spike like interface, whereas $\Delta E_c < 0$ as Type-II or cliff like interface. In Figure 1.10 the schematic band diagram of a $CuInSe_2$/CdS and a $CuInS_2$/CdS interface are plotted. The isotype CdS/ZnO junction is also shown but it is not discussed here due to its minor influence on the diode characteristics. The diagrams are based on current data of the band gap values and the valence band off-set ΔE_v as given by Hengel [45]. It has to be noted, however, that there is still considerable scatter in the literature values of ΔE_v usually determined by Photo Electron Spectroscopy. Nevertheless, general agreement has been reached on the fact that low band gap absorber layers, i.e. $E_g < 1.3$ eV, such as $CuInSe_2$, exhibit a spike-like conduction band discontinuity at the chalcopyrite/CdS interface, whereas high band gap absorbers, such as $CuInS_2$, tend to

show a cliff like discontinuity.

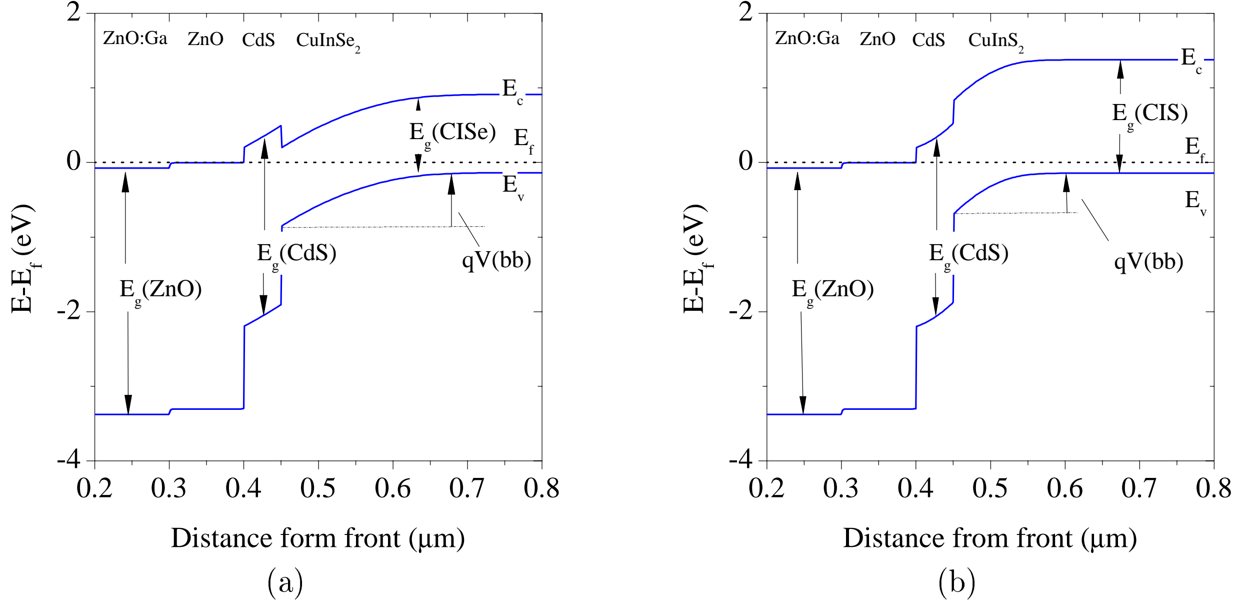

Figure 1.10: Band line up of a chalcopyrite/CdS interface in a (a) $CuInSe_2$/CdS/ZnO structure (type I heterojunction) and a (b) $CuInS_2$/CdS/ZnO structure (type II heterojunction). $qV_{(bb)}$ refers to the maximum band bending at the interface.

1.2.2 Open Circuit Voltage

The attainable open circuit voltage of a specific device structure is governed by recombination in the bulk of the absorber material (space charge region (SCR) or neutral zone) or at the absorber buffer interface. The different recombination paths in a generic heterojunction are indicated in Figure 1.11. In an absorber/window device structure bulk recombination in the window layer can be neglected due to its high band gap. In contrast to Shockley's *ideal* diode, in thin film devices where the width of the space charge region, the width of the neutral zone, and the carrier diffusion length are of the same orders of magnitude recombination processes in the space charge region can not be neglected anymore. In fact, these recombination processes dominate over the recombination in the neutral zone in thin film solar cells. Without going into the details, this can be understood when considering the recombination rate R, which can be approximated by [7]

$$R = \frac{np}{\tau(n+p)}\,, \tag{1.6}$$

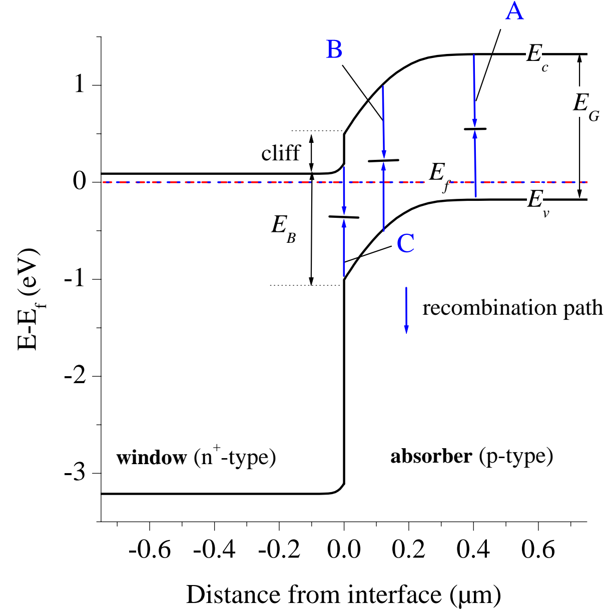

Figure 1.11: Recombination paths at a generic heterojunction. The plotted recombination paths refer to (A) recombination in the neutral zone, (B) recombination on the space charge region, (C) recombination at the interface (redrawn from [46]).

where n and p denote the electron and hole concentration, respectively, and where τ is the carrier life time. The product np, given by

$$np = n_i^2 \exp\left(\frac{qV}{kT}\right) , \qquad (1.7)$$

is nearly constant within the space charge region, hence, according to Equation 1.6 the recombination rate has its maximum where $n = p$, or approximately where $E_f = (E_v{+}E_c)/2$, and it decreases rapidly elsewhere. Recombination losses are effectively avoided if in regions of high recombination velocities, such as the absorber/buffer interfaces, the Fermi-level is either close to the conduction band or close to the valence band [7]. In accordance with this considerations chalcopyrite based solar cells with low band gap absorbers (Type I interface, Figure 1.10 (a)) are dominated by bulk (SCR) rather than interface recombination. However, in the case of a cliff in the conduction band at the junction interface recombination may become dominant because electrons from the window will recombine with holes from the absorber and the carrier densities at the interface have to be described by $E_g - \Delta E_c$ rather than E_g. Thus the spike in the conduction band of the $CuInSe_2$/CdS heterojunction (Figure 1.10 (a)) is more optimal in terms of reducing losses due to interface recombination, than the respective cliff at the $CuInS_2$/CdS interface.

Approximated analytical solutions for the current transport under the presence of different recombination processes can be found in [4, 36, 45]. The dark j-V characteristics and the open circuit limitation under illumination of a device limited by space charge recombination and by interface recombination are listed in Table 1.2.

With respect to the alloying of $CuInS_2$ with Ga it can be seen that the impact of a Ga-induced widening of the absorber band gap onto the open circuit voltage depends on the dominant recombination mechanism. In the case of an SCR-limited device $\Delta qV_{oc} \propto \Delta E_g$,

Table 1.2: Analytical solutions of j-V characteristics of a p-n junction limited by recombination in the space region or at the absorber/buffer interface (from Ref. [45]).

SCR-recombination	interface recombination
$j(V) = j_0(\exp\frac{qV}{2kT} - 1)$	$j(V) = j_0(\exp(\frac{qV}{kT} - 1)$
$j_0 = j_{00}(\exp\frac{-E_g}{2kT})$ E_g = absorber band gap	$j_0 = qSN_V\exp(\frac{-E_b}{kT})$ $E_b = E_g - \Delta E_c$ $E_b \approx$ barrier height at interface ΔE_c = conduction band discontinuity N_V = density of states in valence band S = interface recombination velocity
$V_{oc} = \frac{E_g}{q} - 2kT\ln(\frac{j_{00}}{j_{ph}})$	$V_{oc} = \frac{E_b}{q} - \frac{kT}{q}\ln(\frac{qSN_V}{j_{sc}})$

hence an increase in absorber band gap will also lead to a higher voltage. The situation is not similarly straightforward in a device dominated by interface recombination, where V_{oc} is limited by the barrier height $E_b \approx E_g - \Delta E_c$ at the absorber/window interface. As a consequence increasing the absorber band gap can, in principle, lead to higher open circuit voltages, but this depends on the particular band line up at the hetero-interface. If the energetic position of the valence band is fixed relative to the buffer an increased absorber band gap will increase ΔE_c thereby leaving E_b and hence the open circuit voltage unchanged. For a cliff-type interface this requires that a wider absorber band gap leads to a shift of the energetic position of the valence band with respect to the buffer conduction band.

Tentatively, these considerations have been made responsible for the correlation of open circuit voltage and absorber band gap in solar cells based on the $CuInSe_2$-$CuGaSe_2$ alloy system ($E_{g,CuInSe_2} = 1.04\,\mathrm{eV}$ – $E_{g,CuGaSe_2} = 1.68\,\mathrm{eV}$) [47]. The valence band offsets of the $CuInSe_2$/CdS and the $CuGaSe_2$/CdS interface are almost the same, as could be shown by theoretical calculation [48] as well as by photoemission core-level spectroscopy [47]. Hence the gallium induced band gap widening leads to a shift of the energetic position of the conduction band only and, assuming that this shift is a linear function of composition x [49], the favorable spike-type band line for low [Ga]/([In] + [Ga]) ratios converts into a cliff-type situation for high [Ga]/([In] + [Ga]) ratios. Once the cliff situation has been reached the device may become dominated by interface recombination. Further alloying with Ga does not significantly increase the interface barrier E_b, so that for high Ga-concentrations the gain in V_{oc} falls behind the band gap increase, which is what is can be seen in Figure 1.12.

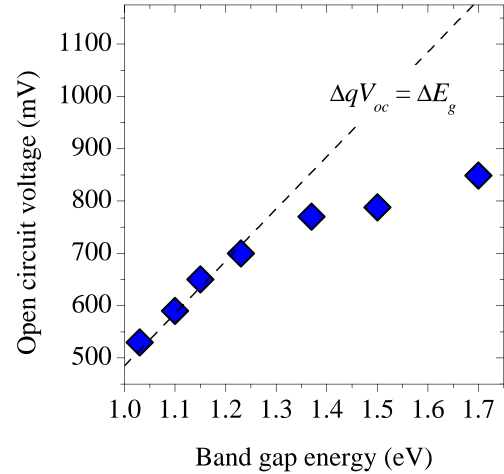

Figure 1.12: Open Circuit Voltage versus absorber band gap of solar cells based on the $CuInSe_2$-$CuGaSe_2$ alloy system (from Ref. [47, 50]).

1.2.3 Spectral Response

A common expression for the spectral sensitivity of a solar cell is the quantum efficiency QE, which describes the fraction of incident photons contributing to the short circuit current density j_{sc} at a given wavelength

$$QE(\lambda) = \frac{1}{q} j_{sc}(\lambda)/n_0(\lambda) \ , \ \text{where} \ \ n_0(\lambda) = I_0(\lambda)\frac{\lambda}{hc} \ . \tag{1.8}$$

Here $n_0(\lambda)$ is the incident photon flux per unit area, $I_0(\lambda)$ stands for the incident light intensity, $j_{sc}(\lambda)$ for the short circuit current density, and all other constants have their usual meaning. In general the quantum efficiency of a device is determined by the fraction of incident photons absorbed within the cell volume, the fraction of those photons absorbed generating electron-hole pairs and the probability that the carriers generated are collected by the p-n junction (collection efficiency). The total photocurrent density under short circuit conditions collected by a solar cell illuminated by monochromatic light may be expressed as:

$$j_{sc}(\lambda) = q \int_0^d n_0(\lambda)[1 - R(\lambda)]G(x)\eta_c(x)dx, \tag{1.9}$$

where, d is the absorber thickness, $R(\lambda)$ is the reflectivity, $G(x)$ is the rate of generation of $e-h$ pairs, and η_c is the collection efficiency. In an ideal case where free-carrier absorption can be neglected each absorbed photon will create an $e-h$ pair, hence $G(x) = -\frac{dn(x)}{dx} = n_0\alpha(\lambda)\mathrm{e}^{-\alpha x}$, where $\alpha(\lambda)$ is the optical absorption coefficient.

An analytical approximation that connects material and device parameters such as absorption coefficients, carrier life times, recombination velocities, etc. can be found in the work of Gärtner [51] or Sze [52]. Klenk and Schock [53] have have used the Gärtner formula for analytical approximations of the photocurrent of $CuGaSe_2$/(Zn,Cd)S heterojunctions. The chosen geometry and boundary conditions are depicted in Figure 1.13 and the quantum

efficiency is given by

$$QE = 1 - \exp(-\alpha_p x_p) \left(\frac{1}{1+\alpha L} - \frac{\alpha L}{\alpha_L^2 L^2 - 1} \frac{\exp(-\alpha \overline{x}) - \exp(-\overline{x}/L)}{\sinh(\overline{x}/L)} \right) , \tag{1.10}$$

where L is the minority carrier diffusion length in the absorber layer and α refers to the absorption coefficient for electron-hole pair generation. Complete collection in the space charge region, no losses at the window/absorber interface, and negligible effects due to light generated majority carriers have been assumed when deriving Equation (1.10). Furthermore, it has to be noted that Equation (1.10) represents an internal quantum efficiency since losses due to reflection and absorption in the window layer have not been taken into account. Mainly due to the wavelength dependence of the absorption coefficient each solar cell region responds differently to incident monochromatic light. This makes spectral response measurements a valuable tool for solar cell device characterization. However, due to the large number of parameters involved the exact knowledge of at least some material parameters is necessary when one wants to extract unknown material parameters from SR measurements.

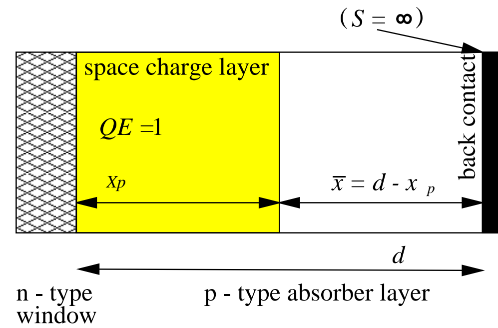

Figure 1.13: Geometry and boundary conditions used in equation 1.10 (from Ref. [53]).

Near band edge spectral response Assuming negligible recombination of photogenerated carries at the back contact (e.g. if $1/\alpha \gg d$) equation 1.10 reduces to

$$QE = 1 - \frac{\exp(-\alpha x_p)}{1+\alpha L} . \tag{1.11}$$

For wavelength just above the absorption edge absorption is still weak and $1/\alpha \gg x_p$ and $1/\alpha \gg L$. Then the denominator of equation 1.11 simplifies to ≈ 1 and the nominator can be expanded into a Taylor-series. Neglecting all high order terms one sees that

$$EQE \approx (\alpha x_p) , \tag{1.12}$$

hence for wavelength just below the cut-off wavelength the EQE is proportional to α. If the spectral dependence of α is known a numerical fit of the EQE data in the weak absorption region can be used to extract the electronic band gap E_g. In the case of chalcopyrite thin film solar cells Phillips [54] has used spectral response measurements to determine the absorber diffusion length and the absorption coefficient around the band edge in $CuInSe_2$ thin film solar cells.

In this work spectral response measurements have been used for determining the band gap of $Cu(In_{1-x}Ga_x)S_2$ layers on grounds of the following considerations. It was shown above that for photon energies just above the absorber band gap energy EQE is proportional to the absorption coefficient α. If the spectral dependence of α is known a fit of the EQE data in the weak absorption region can be used to extract the band gap E_g of the solar cell absorber layer. In a direct band gap material, such as $Cu(In_{1-x}Ga_x)S_2$, the absorption coefficient for photon with energy $h\nu > E_g$ is given by a square-root dependence (see e.g. [55])

$$\alpha(h\nu) = \frac{A}{h\nu}\sqrt{h\nu - E_g}, \quad h\nu > E_g\,, \tag{1.13}$$

where E_g is the band gap of the first direct transition. For $Cu(In_{1-x}Ga_x)S_2$ the constant A is of the order of $1 \times 10^5\,\mathrm{eV}^{1/2}\mathrm{cm}^{-1}$ [56]. Due to this very high absorption coefficient the assumption $1/\alpha \gg d$ is only valid in a very narrow spectral range above the absorption edge. Therefore a direct fit of experimental EQE-data, according to Equation 1.12 is restricted to the same narrow range and is in general not feasible. However, this work mainly considers relative changes in E_g for the band gap of a $Cu(In_{1-x}Ga_x)S_2$ absorber layer is a function of composition x (Figure 1.7). Therefore a quantitative measure of the absorber band gap has been introduced which is based on the first derivative of the EQE. The first derivative of α and hence EQE has a singularity $dEQE/dh\nu \rightarrow \infty$ for $h\nu \rightarrow E_g$. When deriving experimental EQE spectra the singularity at $h\nu = E_g$ will be reflected by a local maximum. Errors due to deviations of the experimental absorption coefficient from Equation 1.13 and due to instrumental broadening influence the spectral position of the maximum, however, it still serves as a good indicator for relative shifts of the absorber band gap E_g.